RSC Advances

PAPER

View Article Online
View Journal | View Issue

Cite this: *RSC Adv.*, 2021, **11**, 35463

Controllable synthesis of N-doped carbon nanohorns: tip from closed to half-closed, used as efficient electrocatalysts for oxygen evolution reaction

Yanli Nan, *[a] Yuanyuan He,[a] Zihan Zhang,[a] Jian Wei[a] and Yubin Zhang*[b]

The development of efficient, cost-effective and stable N-doped carbon material with catalytic activity as an excellent catalyst for the oxygen evolution reaction (OER) is critical for renewable energy systems. In this study, the unique tip-half-closed N-doped carbon nanohorns (THC-N-CNHs) were firstly produced by the positive pressure-assisted arc discharge method using N_2 as the nitrogen source. Benefitting from the novel tip-half-closed structure and sufficient porosity, the specific surface area (SSA) of THC-N-CNHs is calculated to be 670 $m^2 g^{-1}$ without any further treatment, which is three times larger than that of traditional tip-closed CNHs. More importantly, the content of nitrogen can achieve ~1.98 at% with noticeable pyridinic-N enrichment, increasing the number of active sites for the OER. Furthermore, the three-dimensional spherical feature and the unique pore structure for THC-N-CNHs lead to the fast transportation of electrons, and facile release of the evolved O_2 bubbles during the OER process. Therefore, THC-N-CNHs exhibit excellent electrocatalytic activity toward the OER, with an overpotential of 328 mV at 10 mA cm^{-2}, which is superior to that of most N-doped carbon material-based electrocatalysts. Meanwhile, the resulting catalyst also shows excellent durability after long-term cycling. Finally, we emphasize that THC-N-CNHs can be promising candidates as cheap, industrially scalable catalytic scaffolds for OER application.

Received 27th August 2021
Accepted 20th October 2021

DOI: 10.1039/d1ra06458d

rsc.li/rsc-advances

1. Introduction

Oxygen evolution reaction (OER) catalysis constitutes the bottleneck for water splitting, solar cells, metal-air batteries, fuel cells and other renewable energy systems[1–3] due to the sluggish kinetics of the OER, which involves a complex four-electron/proton transfer process.[4,5] Although noble metal oxides like IrO_2 and RuO_2 show excellent catalytic performance for the OER, their widespread development is restricted by their high cost and scarcity.[6–8] Recently, considerable research efforts have been devoted to the development of efficient OER catalysts based on transition metal sulfides and transition metal oxides, such as NiS_2, FeS_2, NiO and so on.[9,10] However, the inherently low conductivity and easy reuniting at the nano-scale after cycling limited their applications for the OER. To solve those problems, the nanoparticles of transition metal sulfides and transition metal oxides are usually supported on conductive substrates such as graphene and carbon nanotubes (CNTs) to enhance the conductivity.[11–16] Previous research also showed that the conductivity of carbon nanomaterials can be improved obviously when adding N atoms into the carbon nanomaterials.[16] Moreover, the N atoms can contribute to the catalytic sites and play synergistic effects between N atoms and metal nanoparticles.[17] However, N-doped graphene is inclined to aggregate or stack hindering the utilization of the active sites and enhancing the transfer resistance after a long-term OER process. In addition, the long length N-doped CNTs enhance the barriers for O_2 releasing and transfer resistance. Based on those considerations, new structure carbon materials should be exploited urgently, which can prevent the aggregation for the nanoparticle catalyst after several cycling, as well as including favorable porosity and N atom doping.

Carbon nanohorns (CNHs) have attracted extensively attention in many research field,[18–20] due to their superior electrical conductivity, the high specific surface area (SSA) after oxidation-treatments, and the optimized nanoporous characteristics. However, studies on N-doped CNHs-based catalysts used for OER are rare, probably limited by the morphological characteristics of the traditional CNHs. Traditional CNHs are constructed by thousands of individual CNH through self-assembling mechanism to form the spherical aggregates with 80–100 nm in diameter.[21,22] The individual CNH tube exhibits the cone-shaped tips presenting closed structure with 40–50 nm in length and 2–3 nm in diameter, distributing pentagonal and heptagonal defects on the tips. In generally, CNHs are formed

[a]*School of Material Science and Engineering, Shaanxi Key Laboratory of Nano Materials and Technology, Xi'an University of Architecture and Technology, Xi'an, 710055, China. E-mail: nanyl@xauat.edu.cn*

[b]*Ningbo University of Finance and Economics, Ningbo, 315175, China. E-mail: zhangyubin@nbufe.edu.cn*

by CO_2 laser evaporation and arc discharge methods.[21,23] Notably, Sano[24,25] *et al.* reported that metal nanoparticles like Pt, Ni, Cu, Zn can be uniformly distributed into the individual CNH tube by modified gas-injected arc-in-water method in N_2, whereas the CNHs have no N atoms doping maybe due to the ionization of nitrogen gas is prohibited by the existence of water. Recently, Qiu[26] *et al.* reported that the large-scale N-doped CNHs can be produced *via* assisted the direct current arc discharge method together with the flowing nitrogen at atmospheric pressure. However, the traditional individual CNH structure for above mentioned CNH is tip-closed structure with low SSA and poor porosity. Although the nanopores created on the tip of individual CNH can be achieved by heat-treatments in O_2 atmosphere or *via* acid treatments due to the "pentagonal" and "heptagonal" defects on CNHs,[27,28] the CNHs and the confined metal nanoparticles produced by one-step arc discharge method will be oxidized, even the structure of CNHs will be destroyed, which are harmful the OER performance.

Herein, adjusting the gas pressure and the ratio of the N_2 and Ar, the unique structure of tip half-closed N-doped CNHs can be produced by positive-pressure assisted arc discharge method, which possess high SSA, optimal pore structure and a large amount of N-doping in natural. Note that, selecting tip-half-closed N-doped CNHs as electrocatalysts for OER were reported for the first time and they show excellent performance for OER. Finally, we proposed that tip half-closed N-doped CNHs would be superior scaffolds based on earth-abundant, scalable, noble-metal-free catalysts for enhancing the performance of OER.

2. Experimental

2.1 Synthesis the CNHs

CNHs were prepared by direct-current arc discharge in positive pressure as reported in previous research.[29] In this work, the reaction conditions are set up at 0.15 MPa in N_2 and Ar mixture atmosphere and 100 A electric current. In detail, an anode and a rod-shaped graphite cathode were set horizontally with 6 and 15 mm in diameter, 15 and 20 cm in length, respectively. The purity of graphite electrode is up to 99.99%. To obtain the stable of the arc plasma the electrode gap was kept at a constant distance ($\sim$2 mm) between the cathode and anode by adjusting the location of the cathode during the plasma process. Three group experiments are obtained in different ratio of N_2 and Ar, which are the Ar in 0.15 MPa, Ar 0.10 MPa and N_2 0.05 MPa, N_2 in 0.15 MPa, respectively. The wall-part products are collected from the chamber. The obtained products are referred to as tip-closed CNHs, tip-half-closed N-doped CNHs (THC-N-doped CNHs), carbon mixture, respectively, with inclusion of the morphologies of the products. Notably, the all-prepared CNHs for these experiments were the level of analytical purity without any further purification and treatment.

2.2 Characterization methods

The transmission electron microscopy (TEM, JEM-2010F) was used to achieve the morphologies of the as-obtained samples. An HR-800 laser confocal micro-Raman spectrometer using laser excitation wavelength of 632 nm was equipped on the Raman spectra. X-ray photoelectron spectrometer (XPS) was collected from the instrument using a monochromatic Al irradiation source (Kratos Axis Ultra DLD), and the C1s peak position at 284.5 eV was used as an internal standard. The SSA and pore size distribution of all samples were measured by N_2 adsorption isotherms condition at 77 K *via* Brauner–Emmett–Teller (BET) methods (Autosorb-1, Quantachrome). By using the field emission scanning electron microscope (FE-SEM) (Gemini, SEM 500), the morphology and EDS mapping for all samples can be obtained.

2.3 Oxygen evolution reaction testing

An electrochemical workstation (CS350, Shanghai Sikete Instruments) was carried out to receive the electrochemical results. All electrochemical measurements were measured by the three-electrode system, using the carbon fiber paper (CFP) coated with the CNH mixture, platinum wire and Hg/HgO (protected by salt bridge) electrode, correspond to the working electrode, the counter electrode, and the reference electrodes, respectively. Briefly, 5 mg of the samples was dissolved with 7 μL of Nafion solution (5%) as binder, and 300 μL of ethanol ultrasonically for 30 min to acquire well dispersion in the solution. The produced CNH mixture was coated onto the CFP with a spatula in 1 cm × 1 cm, then dry them at 80 °C for 30 min in a vacuum oven. The mass loading on the CFP was about 2.5 mg cm^{-2}.

The polarization curve was obtained by consecutive linear sweep voltammetry (LSV) at 5 mV s^{-1} until there is no obvious variation. The 100 mL of 1 M KOH solutions at atmospheric environment is used as the electrolyte solution. According to the LSV curves by plotting overpotential against log(current density), Tafel slopes can be calculated. Electrochemical impedance spectroscopy (EIS) was carried out at 5 mV between 0.01 Hz and 100 kHz. By taking continuous cyclic voltammetry curve (CV) for 2000 cycles, the long-term stability can be evaluated by comparing value of LSV curves before and after cycling at same density current. 80% iR-corrected was applied for all polarization curves.

3. Results and discussion

3.1 The nanostructures of N-doped CNHs

The traditional morphology of the as-grown CNHs with a diameter $\sim$100 nm is shown in Fig. 1(a), which are synthesized in 0.15 MPa Ar by positive pressure assisted arc discharge. The CNHs consist of tubular CNH structures with cone-closed caps observed by HRTEM in Fig. 1(b), also named as tip-closed CNHs at here, which is consistent with the structure of previous reported dahlia-like CNHs.[30] Noticeably, the pentagon and heptagon are the necessary condition to form the cone-cape structure. The model diagrams for overall structure of CNHs, the top view and front view of the individual CNH are illustrated in Fig. 1(c), (g) and (l). The pentagon and heptagon are marked by the orange color in Fig. 1(g) and (1). Interesting, adding a little amount N_2 (0.05 MPa) into the arc furnace cavity, the

morphology of the produced has a significant diversification compared to the tip-closed CNHs as illustrated in Fig. 1(d) and (e). The periphery of CNH exhibits half curled state at tips, which is similar to the few-layer graphene structure confirmed by the interlayer spacing (~0.35 nm) for the graphene layer as depicted in Fig. 1(f). Herein, this production is referred to as the tip half-closed N-doped CNHs (THC-N-CNHs). It should be emphasized that the structure for the rest body of THC-N-CNHs is similar to the tip-closed CNHs. The schematic diagram in Fig. 1(i) makes a vivid description for the individual THC-N-CNH. From the SEM image in Fig. 1(h), we can see that the THC-N-CNHs is also a typical spherical aggregate. The elements of C, O and N are consistently appeared in the THC-N-CNHs (Fig. 1(i–k)) obtained *via* EDX. However, when the arc furnace is fully filled with 0.15 MPa N_2, the production become the carbon mixture, including amorphous carbon, few CNHs as depicted in Fig. 1(j).

Two markedly peaks referred to as D and G bands at ~1351 and ~1582 cm^{-1} are appeared simultaneously for tip-closed CNHs and THC-N-CNHs as depicted in Fig. 2. The G band represents the phonon vibrations in sp^2 carbon materials caused by a normal first-order Raman scattering process. The intensity of D band can be affected by the structural defects.[31] On the basis of the empirical law named Tuinstra and Koenig equation, the nanocrystalline size or defect density for graphitic nanostructures can be obtained by the ratio of I_D and I_G.[32,33] As illustrated in Fig. 2, with increased the N-doping amount, the ratio of I_D and I_G decreases from 1.2 to 0.9, suggesting that the less defects exist on the THC-N-CNH. It should be noted that the result is against to the common scene, the more hetero-atoms doping the more defect degree. It is well known that pentagonal and heptagonal defects are the essential condition to form the cone-shaped cap for CNHs. This result suggests that with increased the N-doping content, the cone-shaped cap structure for CNHs tends to transform the plane structure, which is in agreement with the HRTEM observation. Moreover, the 2D peak become protruding for THC-N-CNHs in contrast to tip-closed CNHs, revealing that the part structure of THC-N-CNH is similar to the graphene sheets.[34]

The N-doping amount and chemical bonding types of the radical composition for all samples can be measured by XPS. In this experiment, three major peaks appearing at ~284.5, ~399.5 and ~533 eV can be denoted as C 1s, N 1s and O 1s as shown in Fig. 3(a), respectively. The content of N atom from THC-N-CNH is calculated to be 1.98 at%. As depicted in Fig. 3(b), the N peak can be divided into three peaks, the peaks at 401.1 eV, 399.4 eV and 397.9 eV correspond to the graphitic-N, pyrrolic-N and pyridinic-N structures. Interestingly, in our case the pyridinic-N content is predominant holding 57%, suggesting that N atoms are linked with two coordinated C atoms at the defect and edge on CNHs. 22% N atoms are connected with two C atoms to form the five-membered ring, and the graphitic-N only occupy 19%. Although the N-doping amount is less than 2 at%, electrocatalytic performance can be significantly improved, attributing to the unique distribution of N-configuration, which will be discussed later in detail. The peak of O 1s can be fitted only one single peak at 532.5 eV as shown in Fig. 3(c), which is attributed to oxygen adsorbed on the surface aroused by exposure in air for THC-N-CNHs and Tip-closed CNHs.[13,35,36]

The adsorption/desorption isotherms of N_2 at 77 K for the tip-closed CNHs and THC-N-CNHs are depicted in Fig. 4(a). In this surface area analysis, the values of SSA for the tip-closed CNHs and THC-N-CNHs are calculated to be 139 $m^2 g^{-1}$, and 663 $m^2 g^{-1}$, respectively. SSA of the THC-N-CNHs is significantly larger than that the tip-closed CNHs increased by 476%. It should be noted that the tip-half closed structure significantly enhance the SSA, which is comparable to the oxidized CNHs at 550 °C in air as reported in previous research.[27]

The pore size distributions of the micropore and mesopore are calculated by the method proposed by Dollimore and Heal[37] on the tip-closed CNHs and THC-N-CNHs, respectively, as illustrated in Fig. 4(b). The main-peak position of micropore of THC-N-CNHs is similar to the tip-closed CNHs, which locates at ~0.6 nm being consistent with the width of interstitial spaces. It can be inferred that the internal spaces of the CNH tubes with tip half-closed structure is the major contributor for SSA, but interstitial micropore plays a relatively small contributor for SSA. There is no obviously peak for tip-closed CNHs range from 2–5 nm as depicted in Fig. 4(c). It should be recognized that the protruding peak at 3–4 nm for THC-N-CNHs are identical to the diameter of the individual CNH owning to the half-closed structure at tips distributing on the periphery for CNHs.

3.2 The formation mechanism of THC-N-CNHs

As previous reported, the arc temperature field during arc discharge process can be distributed from 500–5500 K as shown in Fig. 5(a) and the growth mechanism for the traditional CNHs can be summarized as following.[29] The graphite of anode can be sublimated into the C atoms and small carbon clusters above 5500 K; during 3000–5000 K, the small carbon clusters and carbon atoms get together to form the graphene sheets; then CNHs are formed by the curled graphene sheets into the during 2000–3000 K. The result confirmed that by controlling the duration of graphene sheets and carbon clusters at 2000–3000 K is the critical parameter for synthesis the traditional tip-closed CNHs.

In this experiment, by introducing positive pressure and a little amount of N_2 during arc discharge process, the periphery of CNHs with tip-closed structure turns into the tip-half-closed structure. Moreover, N atoms contents can be obtained to be 1.98 at%. In comparison with the previous reports, Sano[38] *et al.* reported that CNHs can be synthesized by arc-in-water method in N_2, whereas the CNHs have no nitrogen doping. Although Qiu[26] *et al.* reported that the large-scale nitrogen doped CNHs can be achieved by arc discharge method in flowing nitrogen at atmospheric pressure, the obtained production is the traditional tip-closed N-doped CNHs. Hence, one can see that N_2 and positive pressure are the essential conditions to form the tip-half closed structure and to involve abundant N atoms doping.

After observation the process of arc discharge, we found that the rate for the evaporation the anode in N_2 (0.05 MPa) and Ar (0.10 MPa) mixture gas is nearly three times faster than that the purity Ar (0.15 MPa). It is to say that the process of arc discharge

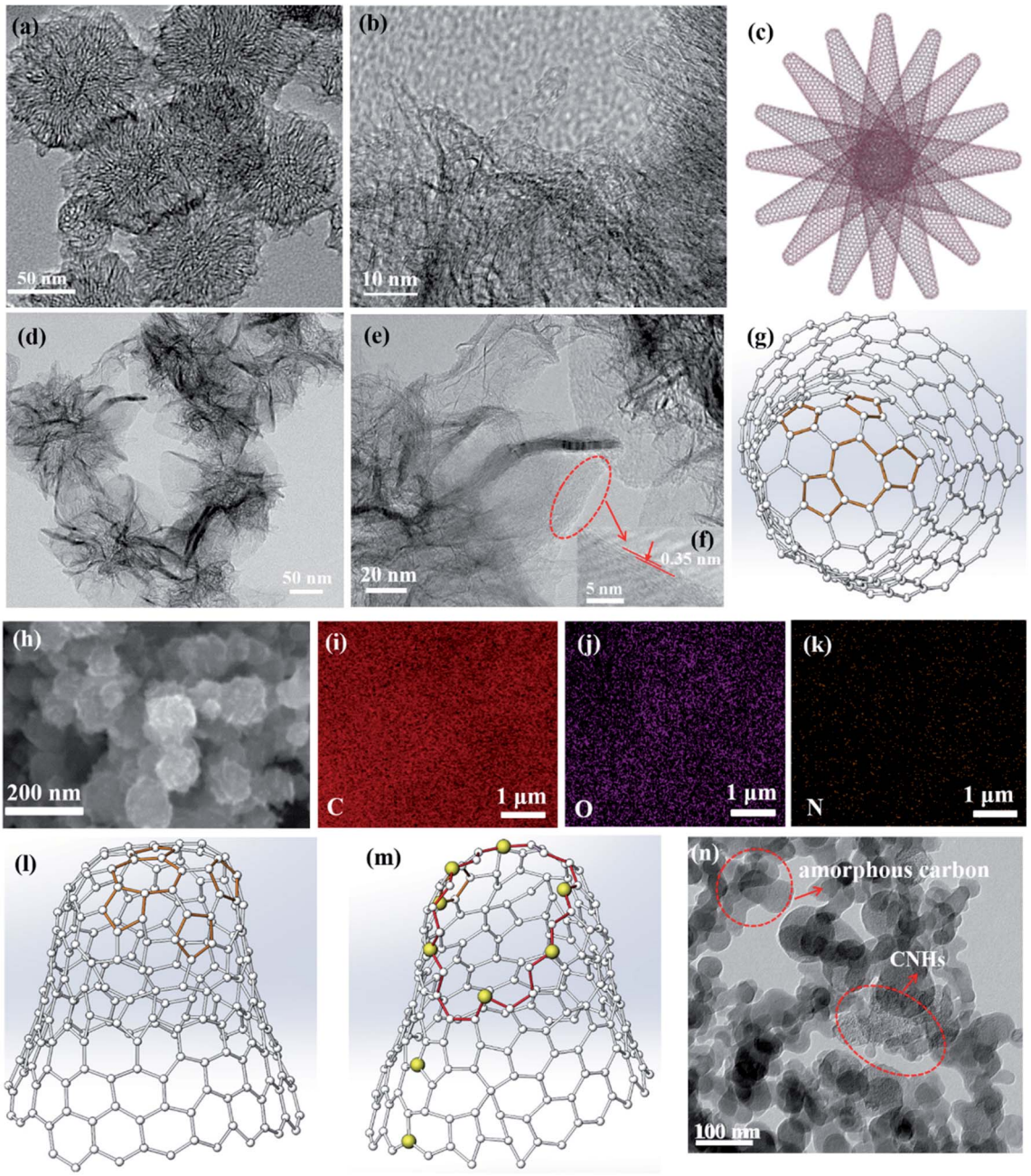

Fig. 1 The TEM (a) and HRTEM (b) images for tip-closed CNHs prepared in Ar atmosphere at 0.15 MPa; the TEM (d) and HRTEM (e), (f) images for THC-N-CNHs prepared in Ar and N_2 atmosphere, 0.10 MPa and 0.05 MPa; the (h) SEM image of the THC-N-CNHs; (i–k) the elemental mapping images for THC-N-CNHs; the schematic diagram for (c) overall CNHs, (g) the top view and (l) front view of individual tip-closed CNH, (m) individual THC-N-CNHs; (n) the TEM image of carbon mixture synthesized in 0.15 MPa N_2.

last shorter time than that purity Ar when burn same length anode. As results, the diffusion rate graphene sheets and carbon clusters increase sharply at the region of 2000–3000 K, causing their duration and reaction time become shorter. Therefore, there is no enough time to curl the tube structure into the half-closed structure. Notably, N_2 can be decomposed into N atoms above 5000 K, but retain nitrogen molecules at 2000–3000 K. Namely, N atom and C atom only can be combined at region near 5000 K. Therefore, the half-closed structure for the CNH tubes induced the larger amount of N atoms exposing on the edges to form the pyridinic-N as shown in Fig. 5(b). The enrichment of pyridinic-N is consistent with the results of XPS results. To confirm this speculation, the comparison experiment is established, decreasing the gas pressure can increase the diffusion rate based on the previous report.[29] Whereas, in 0.1 MPa Ar atmosphere the prepared production mainly focuses on the amorphous carbon, only retained a few tip-half closed CNHs as depicted in Fig. 2(h). Known from this, N_2 is

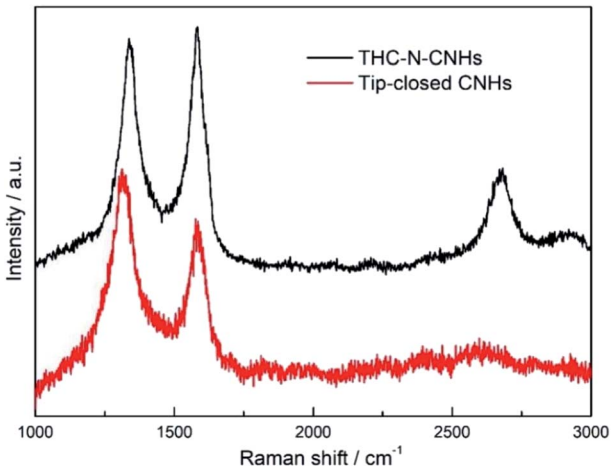

Fig. 2 Raman spectra of tip-closed CNHs and THC-N-CNHs.

indispensable condition to synthesize the THC-N-CNHs for positive pressures assisted arc discharge. When the buffer gas is all instead by N_2, a consideration number of the production are changed to the amorphous carbon, and other carbon materials as shown in Fig. 1(h). In other words, sufficient reaction time is another vital parameter to form the tip-half closed N-doped CNHs.

Above all, we propose that the morphology of THC-N-CNHs can be constructed by introducing the heterogeneous atoms and controlling the reaction time at the region of 2000–3000 K.

3.3 The electrocatalytic activity for THC-N-CNHs

The electrocatalytic activity towards OER for tip-closed CNHs, THC-N-CNHs and RuO_2 was evaluated by a three-electrode chemical station. As summarized in Fig. 6(a), a low overpotential of 328 mV can drive the current density of 10 mA cm^{-2}, slightly higher than that of RuO_2. In contrast, the undoped tip-closed CNHs hardly have catalytic activity, indicating that N-doping in CNHs significantly improve the OER activity. Compared to the behaviors of other nano-carbon catalysts like N-doped CNTs, N-doped graphene,[39,40] this overpotential is more favorable. Contributing to the unique spherical construction, high conductivity and N-doping for THC-N-CNHs, the reaction at electrolyte/electrode interface can be accelerated and the charge transport capability can be improved significantly during the OER process. Specially, the N introduced in the CNHs was predominantly pyridinic-N, which could donate the electron to the π-bond,[41,42] attracting electrons acted as electrocatalytic active sites.

Based on the LSV curves, the Tafel slopes can be evaluated to investigate the OER kinetics for all samples. The much lower Tafel slope for THC-N-CNHs (101.5 mV dec^{-1}) slightly larger

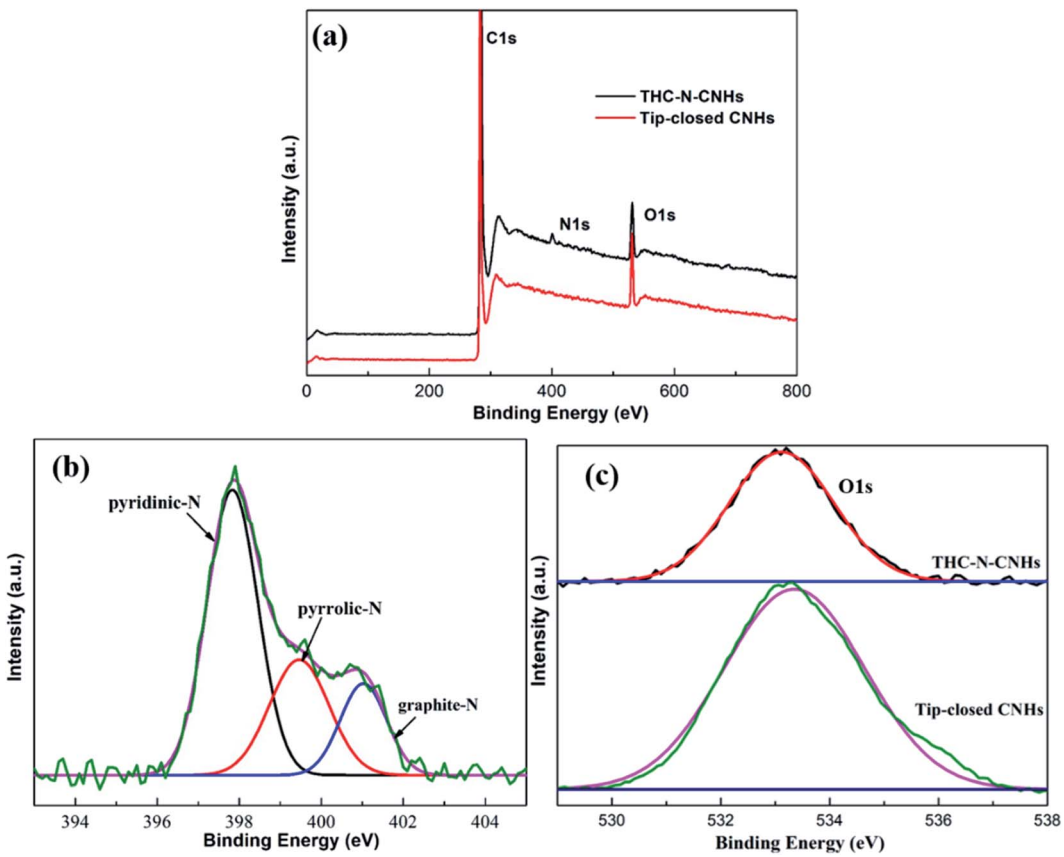

Fig. 3 (a) The XPS spectra of THC-N-CNHs and tip-closed CNHs; (b) the high-resolution of N 1s peak from THC-N-CNHs; (c) the high-resolution of O1s peaks from THC-N-CNHs and tip-closed CNHs.

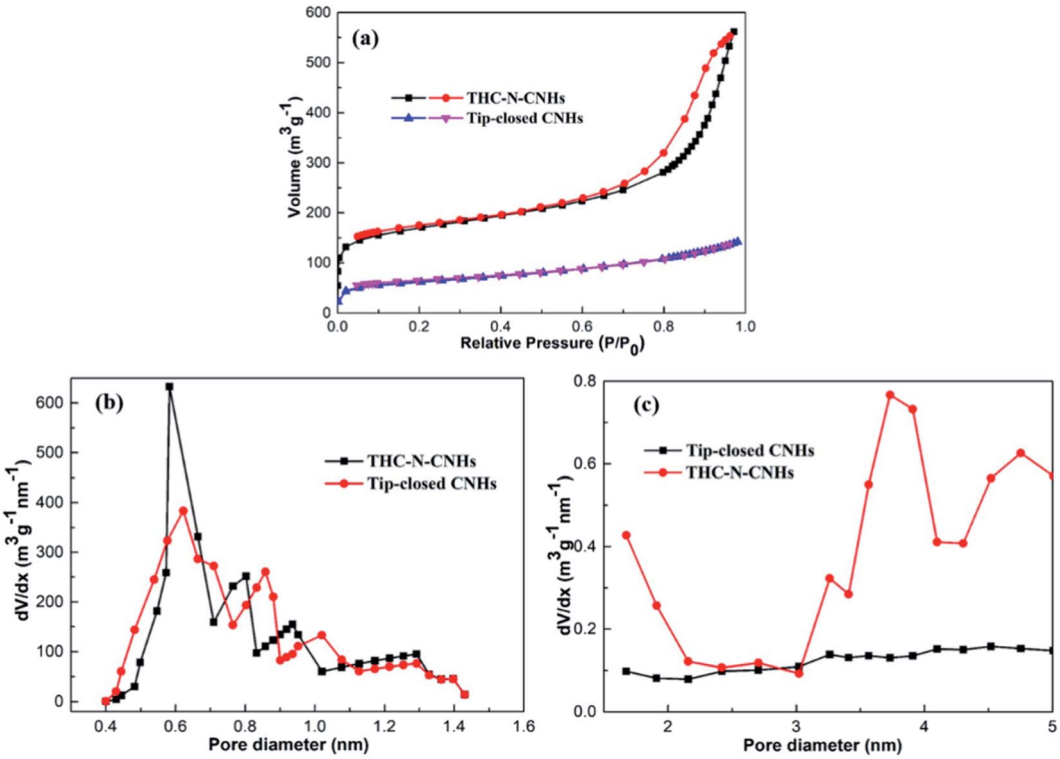

Fig. 4 (a) N_2 adsorption (open symbols) and desorption (filled symbols) isotherms at 77 K of tip-closed CNHs and THC-N-CNHs; (b) the micropores and (c) mesopores size distribution for tip-closed CNHs and THC-N-CNHs.

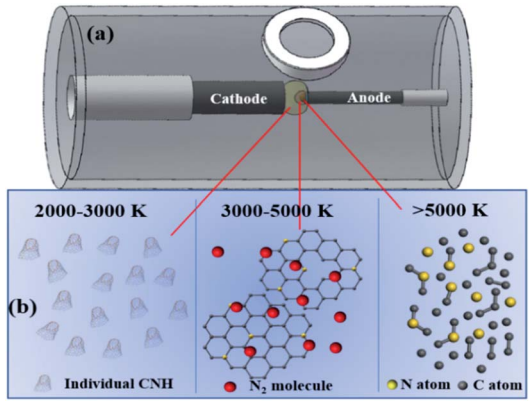

Fig. 5 (a) Schematic of the arc discharge equipment and the temperature distribution of arc torch; (b) region above 5000 K, 3000–5000 K, and 2000–3000 K.

than that RuO_2 (91.0 mV dec^{-1}) reveals appropriate kinetic and superior catalytic activity (Fig. 6(b)).

The electron transfer rate between the catalyst/electrolyte interface can be analyzed by EIS measurements.[43,44] In generally, the diameter of Nyquist plot with a semicircle characteristic indicates the value of charge-transfer resistance (R_{ct}), the smaller R_{ct}, the more favorable electrocatalytic kinetics. The Rct value of THC-N-CNHs is 9 Ω, which is much smaller than that of tip-closed CNHs (16 Ω), suggesting THC-N-CNHs holds much more efficient electron transfer and better catalytic activity during OER process than that of tip-closed CNHs, as shown in Fig. 6(c).

To evaluate the long-term durability, 2000 cycles CV scanning tests were carried out. The value of the overpotential become slight larger than that the initial LSV curve after 2000 CV cycles, which exhibit outstanding electrocatalytic durability for OER, as displayed in Fig. 6(d). From Fig. 6(e), we can see that the structure of most THC-N-CNHs can't be damaged, but a small part of THC-N-CNHs was broken up to a small carbon sheet, indicating that THC-N-CNHs have excellent structural stability.

4. Conclusion

In summary, the catalyst-free and cost-effective synthesis of N-doped CNHs with novel tip half-closed structure and high SSAs in naturally were successfully fabricated *via* arc discharge by employing positive pressure and N_2. The experimental results show that the growth mechanisms for THC-N-CNHs is not only related to the reaction time at 2000–3000 K, but also the composition of the gas above 5000 K for arc temperature. The N atom contents can be achieved to 1.98 at% with enrichment of pyridinic-N. Under 1 M KOH solution, the THC-N-CNHs acquired a low overpotential of 328 mV at 10 mA cm^{-2} and Tafel slope of 101.5 mV dec^{-1}, slightly larger than that the precious metals RuO_2. THC-N-CNHs rendered the promising electrocatalytic activity, attributing to the large SSAs, adequate porosity, N-doping, structural stability and unique tip half-

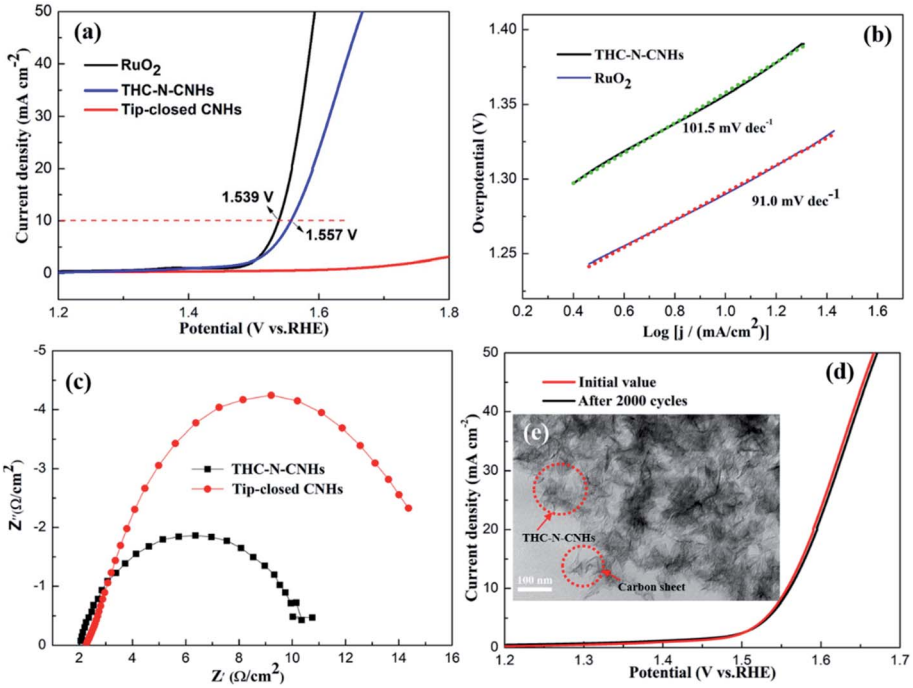

Fig. 6 (a) The OER currents of THC-N-CNHs, tip-closed CNHs, and RuO_2 electrodes in 1 M L^{-1} KOH solution at a scan rate of 5 mV s^{-1}; (b) Tafel plots of commercial RuO_2, THC-N-CNHs; (c) the Nyquist plots of Tip-closed CNHs and THC-N-CNHs; (d) polarization curves for THC-N-CNHs before and after 2000 CV cycles; (e) the TEM image of THC-N-CNHs after 2000 CV cycles.

closed structure. Those result indicate that THC-N-CNH can be a potential candidate as catalyst and a supporting carrier for metal nanoparticles during OER process.

Conflicts of interest

There are no conflicts to declare.

Acknowledgements

This work was funded by China Postdoctoral Science Foundation (Grant No. 2020M683671XB).

References

1 N. T. Suen, S. F. Hung, Q. Quan, N. Zhang, Y. J. Xu and H. M. Chen, Electrocatalysis for the oxygen evolution reaction: recent development and future perspectives, *Chem. Soc. Rev.*, 2017, **46**, 337–365.
2 A. Karmakar, K. Karthick, S. S. Sankar, S. Kumaravel, R. Madhu and S. Kundu, A vast exploration of improvising synthetic strategies for enhancing the OER kinetics of LDH structures: a review, *J. Mater. Chem. A*, 2021, **9**, 1314–1352.
3 S. Y. Zhao, Y. R. Xue, Z. Q. Wang, Z. Q. Zheng, X. Y. Luan, Y. Q. Gao and Y. L. Li, Nickel-based electrocatalysts for energy-related applications: oxygen reduction, oxygen evolution, and hydrogen evolution reactions, *Mater. Chem. Front.*, 2021, **5**, 4153–4159.
4 Z. Lu, C. Wei, X. M. Liu, Y. Y. Fang, X. B. Hao, Y. P. Zang, Z. B. Pei, J. Y. Cai, Y. S. Wu, D. Niu, A. Mosallanezhad, D. Sun, J. Ye, S. W. Niu and G. M. Wang, Ni_2P as a Janus catalyst for water splitting: the oxygen evolution activity of Ni_2P nanoparticles, *Mater. Chem. Front.*, 2021, **5**, 6092–6100.
5 B. R. Xia, T. T. Wang, X. D. Jiang, J. Li, T. M. Zhang, P. Xi, D. Q. Gao and D. S. Xue, N^+-ion irradiation engineering towards the efficient oxygen evolution reaction on NiO nanosheet arrays, *J. Mater. Chem. A*, 2019, **7**, 4729–4733.
6 Y. Yang, Y. K. Kang, H. H. Zhao, X. P. Dai, M. L. Cui, X. B. Luan, X. Zhang, F. Nie, Z. T. Ren and W. Y. Song, An interfacial electron transfer on tetrahedral $NiS_2/NiSe_2$ heterocages with dual-phase synergy for efficiently triggering the oxygen evolution reaction, *Small*, 2020, **16**, 1905083–1905090.
7 S. Mao, Z. Wen, T. Huang, H. Yang and J. Chen, High-performance bi-functional electrocatalysts of 3D crumpled graphene-cobalt oxide nanohybrids for oxygen reduction and evolution reactions, *Energy Environ. Sci.*, 2014, **7**, 609–616.
8 J. Li, P. Liu, J. Mao, J. Yan and W. Song, Two-dimensional conductive metal-organic frameworks with dual metal sites toward the electrochemical oxygen evolution reaction, *J. Mater. Chem. A*, 2021, **9**, 1623–1629.
9 W. Zhou, X. J. Wu, X. Cao, X. Huang, C. Tan, J. Tian, H. Liu, J. Wang and H. Zhang, Ni_3S_2 nanorods/Ni foam composite electrode with low overpotential for electrocatalytic oxygen evolution, Energ, *Environ. Sci.*, 2013, **6**, 2921–2924.
10 S. E. Shaner, R. C. Masse, N. J. Porubsky, S. S. Stahl and J. B. Gerken, A survey of diverse earth abundant oxygen evolution electrocatalysts showing enhanced activity from

Ni-Fe oxides containing a third metal, *Energy Environ. Sci.*, 2014, **7**, 2376–2382.

11 X. Zhang, C. Li, T. Si, H. Lei, C. Wei, Y. Sun, T. Zhan, Q. Liu and J. Guo, FeNi cubic cage@N-doped carbon coupled with N-Doped graphene toward efficient electrochemical water oxidation, *ACS Sustainable Chem. Eng.*, 2018, **6**, 8266–8273.

12 G. Murdachaew and K. Laasonen, Oxygen evolution reaction on nitrogen-doped defective carbon nanotubes and graphene, *J. Phys. Chem. C*, 2018, **122**, 25882–25892.

13 B. Geng, F. Yan, L. N. Liu, C. L. Zhu, B. Li and Y. J. Chen, Ni/MoC heteronanoparticles encapsulated within nitrogen-doped carbon nanotube arrays as highly efficient self-supported electrodes for overall water splitting, *Chem. Eng. J.*, 2021, **406**, 126815.

14 L. N. Liu, X. Zhang, F. Yan, B. Geng, C. L. Zhu and Y. J. Chen, Self-supported N-doped CNT arrays for flexible Zn-air batteries, *J. Mater. Chem. A*, 2020, **8**, 18162–18172.

15 L. N. Liu, Y. Wang, F. Yan, C. L. Zhu, B. Geng, Y. J. Chen and S. L. Chou, Cobalt-encapsulated nitrogen-doped carbon nanotube arrays for flexible zinc–air batteries, *Small Methods*, 2019, **4**, 1900571.

16 Y. Qiu, X. Zhang and S. Yang, High performance supercapacitors based on highly conductive nitrogen-doped graphene sheets, *Phys. Chem. Chem. Phys.*, 2011, **13**, 12554–12558.

17 S. Chen, J. J. Duan, J. R. Ran, M. Jaroniec and S. Z. Qiao, N-doped graphene film-confined nickel nanoparticles as a highly efficient three-dimensional oxygen evolution electrocatalyst, Energ, *Environ. Sci.*, 2013, **6**, 3693–3699.

18 A. G. Pandolfo and A. F. Hollenkamp, Carbon properties and their role in supercapacitors, *J. Power Sources*, 2006, **157**, 11–27.

19 K. P. Annamalai, J. P. Gao, L. L. Liu, J. Mei, W. M. Lau and Y. S. Tao, Nanoporous graphene/single wall carbon nanohorn heterostructures with enhanced capacitance, *J. Mater. Chem. A*, 2015, **3**, 11740–11744.

20 A. Izadi-Najafabadi, T. Yamada, D. N. Futaba, M. Yudasaka, H. Takagi, H. Hatori, S. Iijima and K. Hata, High-power supercapacitor electrodes from single-walled carbon nanohorn/nanotube composite, *ACS Nano*, 2011, **5**, 811–819.

21 S. Iijima, M. Yudasaka, R. Yamada, S. Bandow, K. Suenaga, F. Kokai and K. Takahashi, Nano-aggregates of single-walled graphitic carbon nano-horns, *Chem. Phys. Lett.*, 1999, **309**, 165–170.

22 N. Li, Z. Y. Wang, K. K. Zhao, Z. J. Shi, Z. N. Gu and S. K. Xu, Synthesis of single-wall carbon nanohorns by arc-discharge in air and their formation mechanism, *Carbon*, 2010, **48**, 1580–1585.

23 T. Takikawa, M. Ikeda, K. Hirahara, Y. Hibi, Y. Tao, P. A. Ruiz, T. Sakakibara, S. Itoh and S. Iijima, Fabrication of single-walled carbon nanotubes and nanohorns by means of a torch arc in open air, *Phys. B*, 2002, **323**, 277–279.

24 N. Sano, T. Suntornlohanakul, C. Poonjarernsilp, H. Tamon and T. Charinpanitkul, Controlled syntheses of various palladium alloy nanoparticles dispersed in single-walled carbon nanohorns by one-step formation using an arc discharge method, *Ind. Eng. Chem. Res.*, 2014, **53**, 4732–4738.

25 N. Sano, K. Yamada, T. Suntornlohanakul and H. Tamon, Low temperature oxidation of Fe-included single-walled carbon nanohorns in water by ozone injection to enhance porous and magnetic properties, *Chem. Eng. J.*, 2016, **283**, 978–981.

26 L. Sun, C. L. Wang, Y. Zhou, X. Zhang, B. Cai and J. S. Qiu, Flowing nitrogen assisted-arc discharge synthesis of nitrogen-doped single-walled carbon nanohorns, *Appl. Surf. Sci.*, 2013, **277**, 88–93.

27 J. Miyawaki, R. Yuge, T. Kawai, M. Yudasaka and S. Iijima, Evidence of thermal closing of atomic-vacancy holes in single-wall carbon nanohorns, *J. Phys. Chem. C*, 2007, **111**, 1553–1555.

28 J. Fan, R. Yuge, J. Miyawaki, T. Kawai, S. Iijimia and M. Yudasaka, Close-open-close evolution of holes at the tips of conical graphene of single-wall carbon nanohorns, *J. Phys. Chem. C*, 2008, **112**, 8600–8603.

29 Y. L. Nan, B. Li, P. Zhang, S. C. Shen and X. L. Song, Positive pressure assisted-arc discharge synthesis of single-walled carbon nanohorns, *Mater. Lett.*, 2016, **180**, 313–316.

30 Y. L. Nan, B. Li, X. L. Song and N. Sano, Optimization of pore-opening condition in single-walled carbon nanohorns to achieve high capacity in double layer capacitor at high charge-discharge rate: critical effect of their hierarchical pore structures, *Carbon*, 2019, **142**, 150–155.

31 A. Reina, X. T. Jia, J. Ho, D. Nezich, H. B. Son, V. Bulovic, M. S. Dresselhaus and J. Kong, Large area, few-layer graphene films on arbitrary substrates by chemical vapor deposition, *Nano Lett.*, 2009, **9**, 30–35.

32 H. J. Jung, Y. J. Kim, J. H. Han, M. Yudasaka, S. Iijima, H. Kanoh, Y. A. Kim, K. Kaneko and C. M. Yang, Thermal-treatment-induced enhancement in effective surface area of single-walled carbon nanohorns for supercapacitor application, *J. Phys. Chem. C*, 2013, **117**, 25877–25883.

33 T. Yamaguchi, S. Bandow and S. Iijima, Synthesis of carbon nanohorn particles by simple pulsed arc discharge ignited between pre-heated carbon rods, *Chem. Phys. Lett.*, 2004, **389**, 181–185.

34 Z. H. Ni, Y. Y. Wang, T. Yu and Z. X. Shen, Raman spectroscopy and imaging of graphene, *Nano Res.*, 2008, **1**, 273–291.

35 Z. Li, Y. Chen, Y. Xin and Z. Zhang, Sensitive electrochemical nonenzymatic glucose sensing based on anodized CuO nanowires on three-dimensional porous copper foam, *Sci. Rep.*, 2015, **5**, 16115.

36 M. A. Dar, Y. S. Kim, W. B. Kim, J. M. Sohn and H. S. Shin, Structural and magnetic properties of CuO nanoneedles synthesized by hydrothermal method, *Appl. Surf. Sci.*, 2008, **254**, 7477–7481.

37 D. Dollimore and G. R. Heal, An improved method for the calculation of pore size distribution from adsorption data, *J. Appl. Chem.*, 1964, **14**, 109–114.

38 N. Sano, Low-cost synthesis of single-walled carbon nanohorns using the arc in water method with gas injection, *J. Phys. D: Appl. Phys.*, 2004, **37**, 17–20.

39 N. Y. Cheng, Q. Liu, J. Q. Tian, Y. R. Xue, A. M. Asiri, H. F. Jiang, Y. Q. He and X. P. Sun, Acidically oxidized

carbon cloth: a novel metal-free oxygen evolution electrode with high catalytic activity, *Chem. Commun.*, 2015, **51**, 1616–1619.

40 G. L. Tian, M. Q. Zhao, D. S. Yu, X. Y. Kong, J. Q. Huang, Q. Zhang and F. Wei, Nitrogen-doped graphene/carbon nanotube hybrids: *in situ* formation on bifunctional catalysts and their superior electrocatalytic activity for oxygen evolution/reduction reaction, *Small*, 2014, **10**, 2251–2259.

41 Z. Zafar, Z. H. Ni, X. Wu, Z. X. Shi, H. Y. Nan, J. Bai and L. T. Sun, Evolution of Raman spectra in nitrogen doped graphene, *Carbon*, 2013, **61**, 57–62.

42 L. W. Zhang, A. Gao, Y. Liu, Y. Wang and J. T. Ma, PtRu nanoparticles dispersed on nitrogen-doped carbon nanohorns as an efficient electrocatalyst for methanol oxidation reaction, *Electrochim. Acta*, 2014, **132**, 416–422.

43 Y. J. Lei, L. Wei, S. L. Zhai, Y. Q. Wang, H. E. Karahan, X. C. Chen, Z. Zhou, C. J. Wang, X. Sui and Y. Chen, Surface modification of $MnCo_2O_4$ with conducting poly pyrrole as a highly active bifunctional electrocatalyst for oxygen reduction and oxygen evolution reaction, *Mater. Chem. Front.*, 2018, **2**, 102–111.

44 Z. Q. Xue, X. Li, Q. L. Liu, M. K. Cai, K. Liu, M. Liu, Z. F. Ke, X. L. Liu and G. Q. Li, Interfacial electronic structure modulation of NiTe nanoarrays with NiS nanodots facilitates electrocatalytic oxygen evolution, *Adv. Mater.*, 2019, **31**, 19004301–19004307.